ELSEVIER

Journal of Power Sources 53 (1995) 31–43

JOURNAL OF POWER SOURCES

The influence of calcium, tin and grid thickness on corrosion-induced grid growth

Herbert Giess

Accumulatoren Fabrik Oerlikon, 8050 Zurich, Switzerland

Received 25 July 1994; accepted 10 August 1994

Abstract

Antimony-free lead alloys are the choice material for the positive and negative grids of valve-regulated, stationary, lead/acid (VRLA) batteries. A lead alloy suitable for this task is a ternary lead–calcium–tin alloy with additions of aluminium. The influence of two levels of calcium and tin, as well as the grid thickness, on the corrosion rate (i.e., growth) is investigated through tests on bare and pasted grids. The results show that a combination of a low calcium ($\approx$0.07 wt.%) and a high tin ($\approx$0.7 wt.%) content in the alloy, together with thick grids ($\approx$4 mm), yields low growth-rates that are adequate for long-life VRLA batteries (3–6% growth in 54 weeks at +60 °C). The microstructure of the alloy, i.e., the number of grain boundaries per unit volume determines the magnitude of the resulting corrosion attack. Lead–calcium–tin–aluminium alloys with an approximate composition of 0.07 wt.% Ca and 0.7 wt.% Sn have a lower number of grain boundaries when compared with alloys of the same system with 0.09 wt.% Ca and 0.3 wt.% Sn. Although a penetrating grain-boundary attack is observed with the Pb–0.07wt.%Ca–0.7wt.%Sn alloy, its overall performance, in terms of resulting VRLA battery life, is far superior to that of the Pb–0.09wt.%Ca–0.3wt.%Sn alloy.

Keywords: Calcium; Tin; Grid thickness; Corrosion; Lead/acid batteries

1. Introduction

Antimony-free lead alloys are the choice material for the positive and negative grids of valve-regulated, stationary, lead/acid (VRLA) batteries. One family of lead alloys suitable for the task is a ternary lead–calcium–tin alloy with additions of aluminium. The ongoing industry-wide search for enhanced VRLA batteries has required an improvement in the corrosion behaviour of the positive grids and an evaluation of the influence of calcium and tin levels, as well as grid thickness, on the corrosion resistance of such batteries.

Results show that a combination of a low Ca ($\approx$0.07 wt.%) and a high Sn ($\approx$0.7 wt.%) content in the alloy, together with thick grids ($\approx$4 mm), gives a battery service life of $\geqslant$10 years, even at higher average ambient temperatures. This service life was evaluated from an accelerated life test for 54 weeks at 60 °C and a float voltage of 2.28 V/cell. The acceleration factor under these test conditions is assumed to be 16.

2. Experimental

2.1. Grid casting

The grids were produced on industry-standard casters (Wirtz 40C and 330C units) with a casting speed of 9–12 double-panels per minute. The alloy was held at 470 $\pm$ 10 °C and introduced via a ladle (at 430–460 °C) into the grid mold at 120–150 °C. After a residence time of 5–7 s in the mold, the grids (see Fig. 1) were ejected, doused with a water spray, and then left to cool down to room temperature on the caster grid rack. In order to evaluate the reproducibility of the alloy properties, grids were cast during 8 h production runs at several dates and production sites.

2.2. Bare grid corrosion

Experiments were performed on 8–18 replicate single-panel grids for each alloy. To assure uniform test conditions, the bare grids of different composition were stacked in an alternating fashion in a horizontal position and welded to a common lead-alloy bus-bar. The plate

SSDI 0378-7753(94)01974-Z

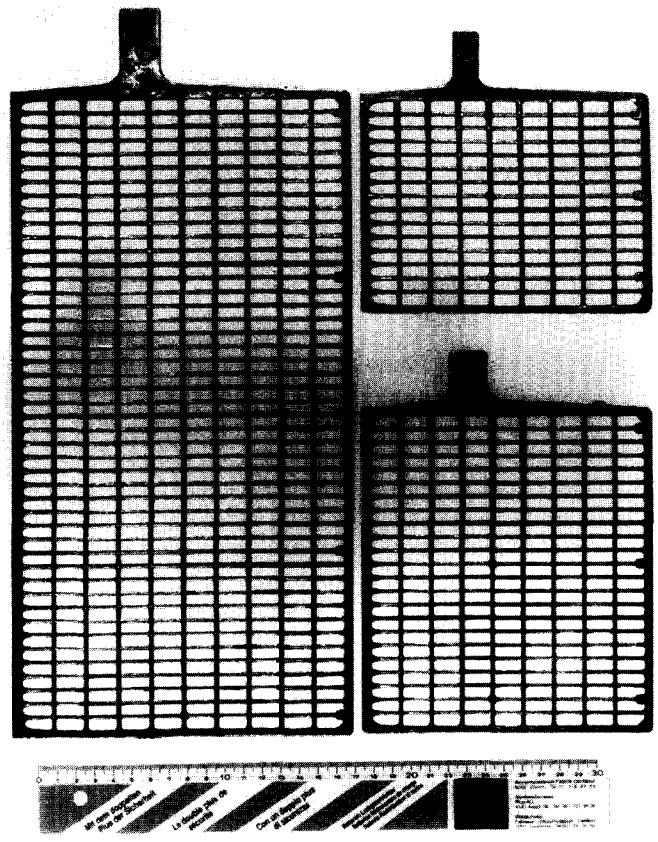

Fig. 1. Grids produced on industry standard casters with a casting speed of 9–12 double-panels per minute.

stack was inserted into a transparent SAN cell jar and operated against a negative plate with a Pb–Ca–Sn alloy grid. The cells were filled with 1.280 sp. gr. sulfuric acid at 20 °C and were kept in a thermostatted water bath with a temperature regulation of ±1 °C.

The corrosion of this positive-grid assembly was conducted under constant-voltage conditions that resulted in a grid potential between +1200 and +1300 mV versus an Hg/Hg_2SO_4 reference electrode held at the same temperature. This potential is similar to the value found for positive plates in VRLA cells on constant-voltage float. After selected time periods, such grid stacks were extracted from the cell jars, washed free of acid, and dried. The grid growth was determined by measuring the maximum horizontal grid width to ±0.01 mm and is reported as the percentage increase over the reference grid width before the experiment (approx. 155 mm).

2.3. Pasted grid corrosion

This experiment was performed with regular 6 V/100 Ah, 2 V/300 Ah and 2 V/450 Ah VRLA cells and monoblocs. The grid alloys selected for this experiment were those giving the extreme values of corrosion behaviour as identified in the bare-grid experiments. The cells and monoblocs were held in thermostatted water baths at 60±1 °C and a constant float voltage of 2.28±0.01 V/cell. The cell cases were individually supported on opposite facing sides with finger-tightened clamps according to BS 6290:Part 4 (revision 5).

The health of the cells was monitored by approximately weekly measurements of the internal resistance, at 60 °C and after less than 5 min of open-circuit stand. This was performed with a Hewlett Packard HP4338A milliohmmeter and coaxial pin probes, on the cell or monobloc terminals. The residual capacity was monitored at adequate intervals with high-rate discharges (10/30 min rate to 1.6 V/cell) at test or room temperature.

2.4. Metallography

Selected grid samples were embedded with an epoxy resin (Epofix Struers) and then prepared metallographically with a final polishing stage using 1 μm diamond paste. A wipe etch with a 2:3 vol./vol. solution of glycerine in ethanol that contained small quantities of HNO_3 and H_2O_2 was used to reveal the alloy microstructures. Microphotographs were taken either with normal illumination or Normaski interference contrast (DIC).

3. Results and discussion

3.1. Compositional analysis

The chemical analysis of the cast grids is presented in Table 1. This shows that, except for the bismuth content, all other analyzed minor elements are present at a concentration below 0.002 wt.%.

3.2. Metallurgical structure

Samples for the determination of the alloy-characteristic microstructure were taken from three locations on the grid, namely: (i) the grid frame at the gate; (ii) the vertical wires of the inner grid members; (iii) the grid frame opposite the gate. The microstructures can be described as follows.

Pb–Ca–Sn–Al (A903) alloy. The microstructure consists of grains of irregular shape and with dimensions that range from 20 to 500 μm (Fig. 2). There is also evidence of nearly complete secondary recrystallization.

Pb–Ca–Sn–Al (A907) alloy. The microstructure consists of irregular-shaped grains with a slight columnar orientation in the direction of the heat flow during solidification (Fig. 3). There is a grain sub-structure with slight 'coring' (due to non-equilibrium solidification) and tin segregation, as well as incomplete secondary recrystallization.

Table 1
Composition (wt.%) of cast grids for selected elements, as determined by spark emission spectroscopy (average of 4 determinations). Sample position: grid lug

Alloy code	Ca	Sn	Al	Sb	As	Cu	Zn	Cd	Bi	Ag	Se	Te	Ni	Fe
A903	0.0914	0.263	0.0185	<0.001	<0.002	<0.001	<0.001	<0.001	0.0072	0.0005	<0.001	<0.001	<0.001	<0.001
A907	0.0868	0.740	0.0233	<0.001	<0.002	<0.001	<0.001	<0.001	0.0071	0.0005	<0.001	<0.001	<0.001	<0.001
A603	0.0650	0.288	0.0228	<0.001	<0.002	<0.001	<0.001	<0.001	0.0075	0.0003	<0.001	<0.001	<0.001	<0.001
A607	0.0605	0.766	0.0233	<0.001	<0.002	<0.001	<0.001	<0.001	0.0074	0.0003	<0.001	<0.001	<0.001	<0.001
A804	0.0815	0.455	0.0139	<0.001	<0.002	<0.001	<0.001	<0.001	0.0028	0.0004	<0.001	<0.001	<0.001	<0.001
A903	0.0927	0.267	0.0237	<0.001	<0.002	<0.001	<0.001	<0.001	0.0069	0.0005	<0.001	<0.001	<0.001	<0.001
A707	0.0753	0.686	0.0096	<0.001	<0.002	<0.001	<0.001	<0.001	0.0076	0.0017	<0.001	<0.001	<0.001	<0.001

Fig. 2. Microstructure of Pb–Ca–Sn–Al (A903) alloy (reference bar 202 μm). Cross section of a triangular, interior wire member of the grid. Variable size, irregular-shaped grains.

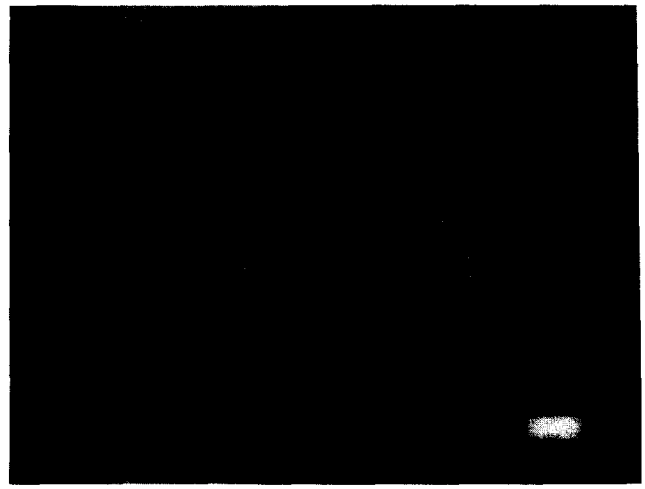

Fig. 3. Microstructure of Pb–Ca–Sn–Al (A907) alloy (reference bar 202 μm). Cross section of a triangular, interior wire member of the grid. Variable size, irregular-shaped grains with slight orientation effects and segregated tin sub-structure.

Pb–Ca–Sn–Al (A603) alloy. The microstructure has a variable-size grain structure that ranges from 20 to 600 μm (Fig. 4). There is slight coring and tin segregation, with little secondary recrystallization.

Pb–Ca–Sn–Al (A607) alloy. Large grains with tin segregation are found in the grain sub-structure (Fig. 5). There are strong grain orientation effects with the formation of linear grain boundaries in the interior of the casting section at the meeting point of the oriented grains. Growth of the grains in the direction of the predominant heat flow.

3.3. Grid growth

The grid growth was determined as the percentage horizontal increase of a ≈155 mm wide grid in a given

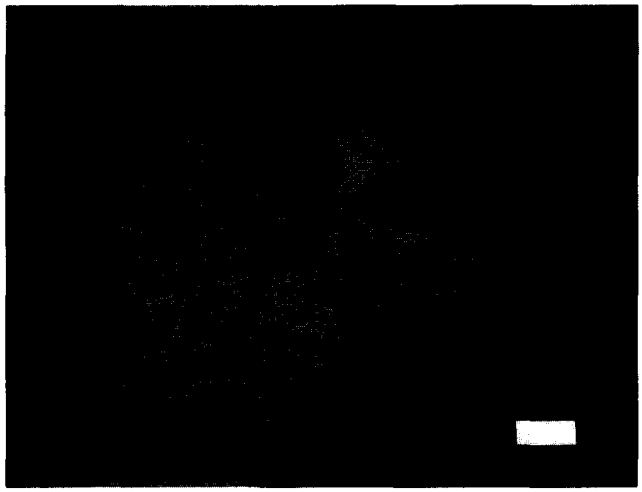

Fig. 4. Microstructure of Pb–Ca–Sn–Al (A603) alloy (reference bar 202 μm). Cross section of a triangular, interior wire member of the grid. Variable size, irregular-shaped grains with slight segregated tin sub-structure.

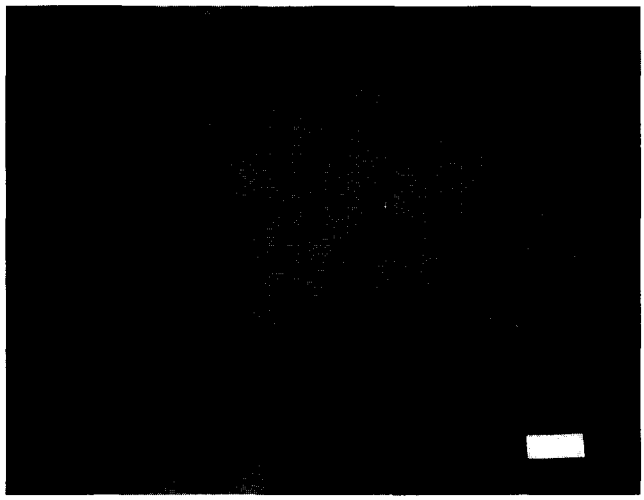

Fig. 5. Microstructure of Pb–Ca–Sn–Al (A707) alloy (reference bar 202 μm). Cross section of a triangular, interior wire member of the grid. Large grains with strong, tin-induced, grain sub-structure and preferred orientation.

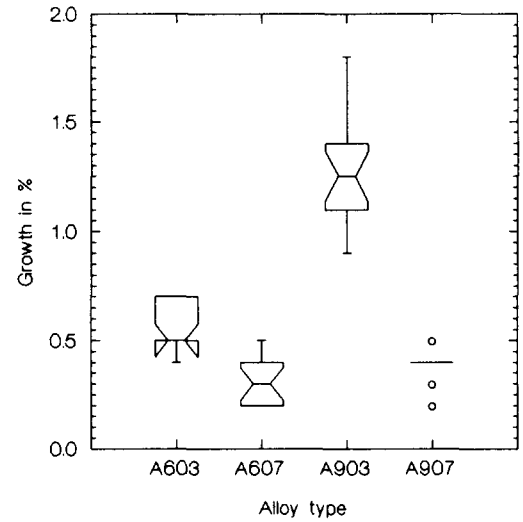

Fig. 6. Notched box plot of grid growth of 18 bare, 4 mm thick, grids for alloys held at +1200 to +1300 mV vs. Hg/Hg_2SO_4 and 80 °C for 6 weeks equivalent to ~7.4 years at 20 °C (box with 95% confidence intervals).

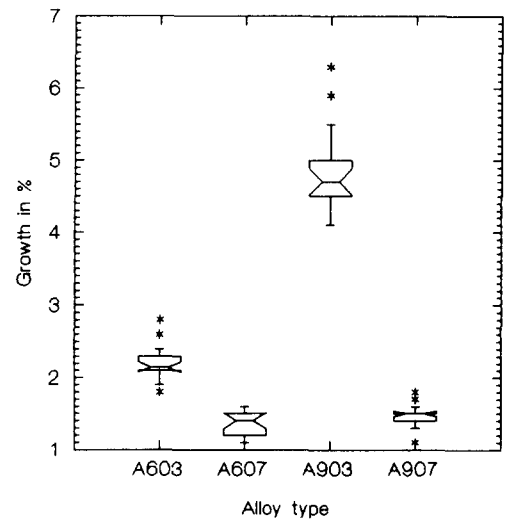

Fig. 7. Notched box plot of grid growth of 18 bare, 4 mm thick, grids for alloys held at +1200 to +1300 mV vs. Hg/Hg_2SO_4 and 80 °C for 12 weeks equivalent to ~14.8 years at 20 °C (box with 95% confidence intervals).

time period at a given test temperature. Grid growth is preferred over weight or cross-sectional area loss data because it appears to be more directly related to discharge performance and to eventual secondary damage of the cell or monobloc container. In the growth measurement, the horizontal growth was used as determined by the largest measured increase in grid width.

A notched box plot [1] presentation of the growth data has been chosen to display the significant differences and scatter of the growth data within an alloy group. In the plot, the notch corresponds to the median of the values and the termination of the box to the 95% confidence interval for the median. Low scatter is desirable as it denotes a small sensitivity of the alloy and resulting grid structure towards irregular corrosion. Non-overlapping box markers indicate significant differences in the growth data of the alloy types (Figs. 6 and 7). For example, in Fig. 7, alloys A607 and A907 show no major difference in growth at the 95% confidence level. The growth of the A603 alloy is, however, statistically significantly different, i.e., it is higher.

In the above experiments, a rather high electrolyte temperature of 80 °C was used. To evaluate if this temperature was influencing the ranking of the corrosion resistance of the tested alloys, a lower temperature corrosion experiment at 50 °C was performed under otherwise identical test conditions. The data of Fig. 8 show that the ranking of the alloys has remained essentially the same. For a shorter time at room tem-

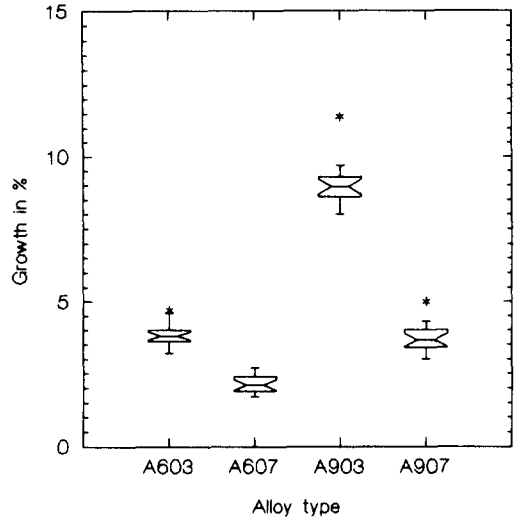

Fig. 8. Notched box plot of grid growth of 18 bare, 4 mm thick, grids for alloys held at +1200 to +1300 mV vs. Hg/Hg_2SO_4 and 50 °C for 54 weeks equivalent to ~8.3 years at 20 °C (box with 95% confidence intervals).

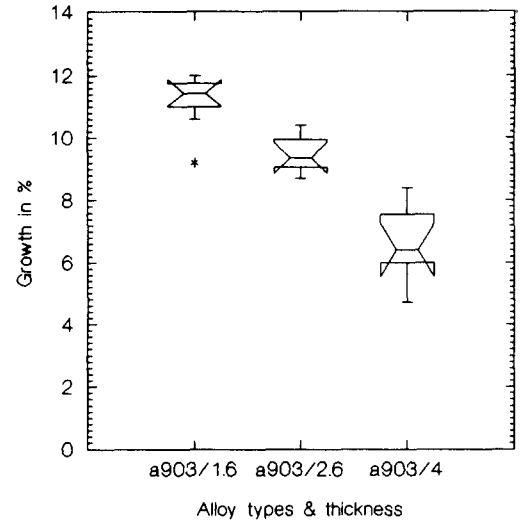

Fig. 10. Notched box plot of grid growth of 8 bare, A903 alloy grids with nominal grid thickness of 4.0, 2.6 and 1.6 mm held at +1200 to +1300 mV vs. Hg/Hg_2SO_4 and 80 °C for 11 weeks equivalent to ~13.5 years at 20 °C (box with 95% confidence intervals).

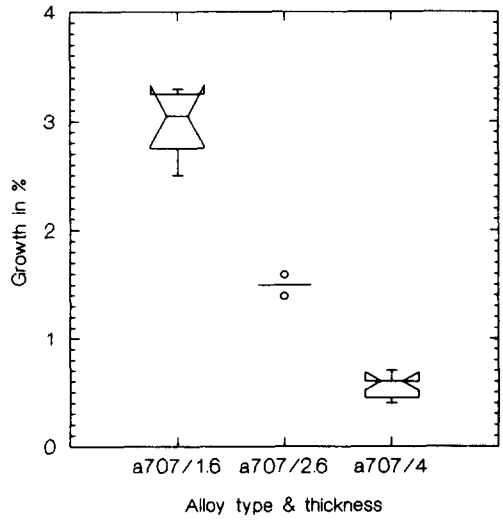

Fig. 9. Notched box plot of grid growth of 8 bare, A707 alloy grids with nominal grid thickness of 4.0, 2.6 and 1.6 mm held at +1200 to +1300 mV vs. Hg/Hg_2SO_4 and 80 °C for 11 weeks equivalent to ~13.5 years at 20 °C (box with 95% confidence intervals).

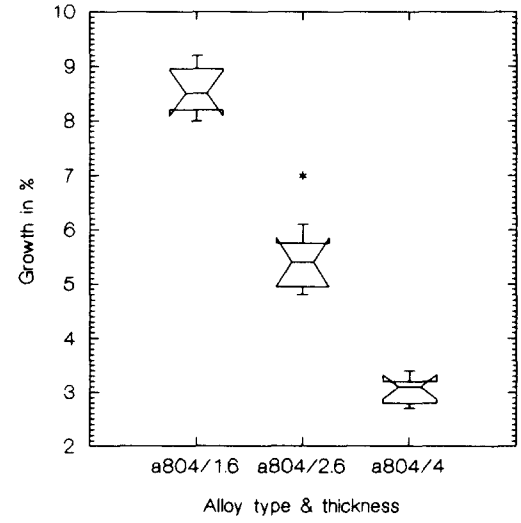

Fig. 11. Notched box plot of grid growth of 8 bare, A804 alloy grids with nominal grid thickness of 4.0, 2.6 and 1.6 mm held at +1200 to +1300 mV vs. Hg/Hg_2SO_4 and 80 °C for 11 weeks equivalent to ~13.5 years at 20 °C (box with 95% confidence intervals).

perature (~8.3 years/20 °C) the absolute amount of growth has been found to be higher than that observed in the 80 °C experiment (~14 years/20 °C). This would indicate that data obtained at very high temperatures give reliable ranking values, but that values of absolute growth may be underestimated in such an experiment.

It can be seen from Figs. 7 and 8 that a decrease in the calcium content from 0.09 to 0.06 wt.% gives a similar improvement in corrosion resistance as an increase in the tin content from 0.3 to 0.7 wt.%. A still superior performance is achieved when both key constituents are modified together (i.e., calcium content decreased, tin content increased). This results from the lower number of grain boundaries present in such an alloy.

The above experiments have been carried out with grids with a nominal thickness of 4 mm. In order to evaluate the effect of grid thickness on the growth rate, experiments were carried out on grids of nearly identical design but with a nominal thickness of 2.6 or 1.6 mm. (Figs. 9–13).

To give a quantitative ranking of the amount of lead and possible strength of the grids of different thickness, a grid design factor was calculated. To obtain this factor the grid weight was divided by the grid thickness resulting in a gram/mm factor as follows:

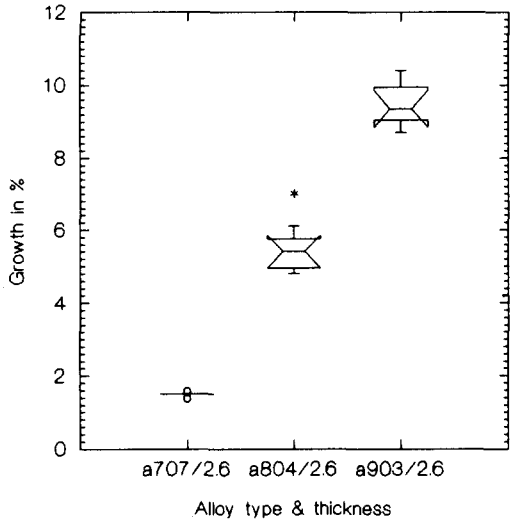

Fig. 12. Notched box plot of grid growth of 8 bare A707, A804 and A903 alloy grids with nominal grid thickness of 2.6 mm held at +1200 to +1300 mV vs. Hg/Hg_2SO_4 and 80 °C for 11 weeks equivalent to ~13.5 years at 20 °C (box with 95% confidence intervals).

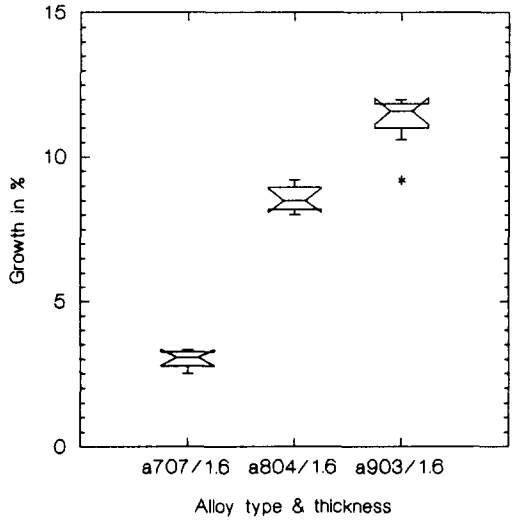

Fig. 13. Notched box plot of grid growth of 8 bare A707, A804 and A903 alloy grids with nominal grid thickness of 1.6 mm held at +1200 to +1300 mV vs. Hg/Hg_2SO_4 and 80 °C for 11 weeks equivalent to ~13.5 years at 20 °C (box with 95% confidence intervals).

1.6 mm, 80 g: 80/1.6 = 50 g mm^{-1}
2.6 mm, 139 g: 139/2.6 = 53 g mm^{-1}
4.0 mm, 237 g: 237/4.0 = 59 g mm^{-1}

This factor shows that the 4 mm grid had approximately 11 and 18% more lead per unit of thickness than the 2.6 mm and the 1.6 mm grid, respectively.

The growth data (Figs. 9–13) of the different grid alloys reveal that low calcium (≈0.07 wt.%)/high tin (≈0.7 wt.%) alloys show better corrosion behaviour and that this behaviour is carried over also into thin grid cross sections. The data presented in Fig. 14 show that a bare 1.6 mm grid cast with the A707 alloy has less corrosion-induced growth than a 4.0 mm grid cast with the A804 alloy or an ~5.5 mm grid cast with the

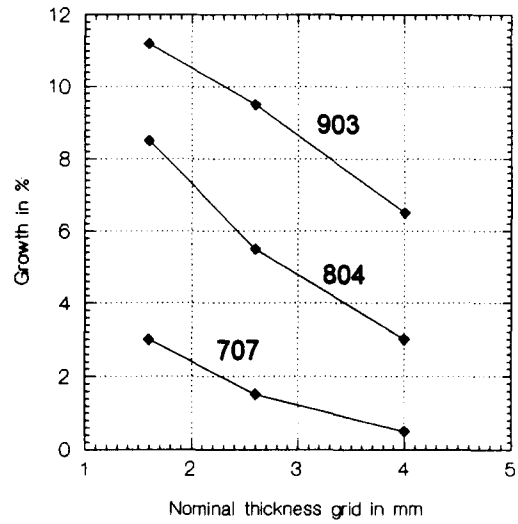

Fig. 14. Plot of grid growth of 8 bare A707, A804 and A903 alloy grids as a function of nominal grid thickness held at +1200 to +1300 mV vs. Hg/Hg_2SO_4 and 80 °C for 11 weeks equivalent to ~13.5 years at 20 °C. Specific grid data: 1.6 mm, 80 g: 80/1.6 = 50 g mm^{-1}; 2.6 mm, 139 g: 139/2.6 = 53 g mm^{-1}; 4.0 mm, 237 g: 237/4.0 = 59 g mm^{-1}.

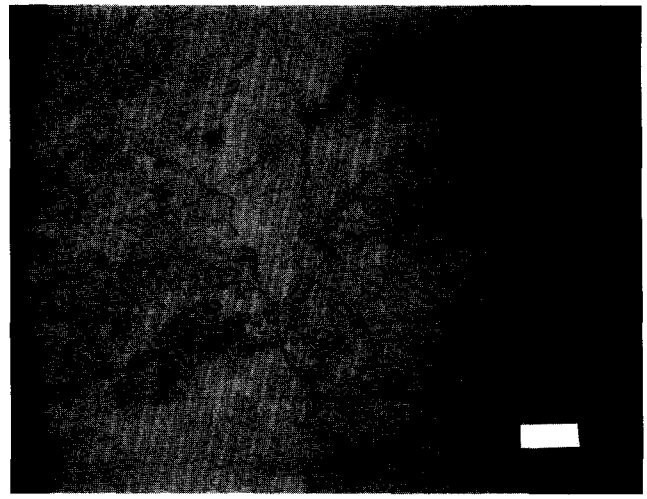

Fig. 15. Microstructure of Pb–Ca–Sn–Al (A707) alloy (reference bar 440 μm). Nominal grid thickness 4 mm. Note presence of linear grain boundaries formed by the meeting of inward growing grains during solidification of the alloy.

A903 alloy. The microstructure/grain size of such grids is presented in Figs. 15–17 and reveals the strong oriented growth of the grains during solidification. This carry-over allays fears that the larger-grained, low calcium/high tin alloys may cause thin grids to be more susceptible to catastrophic corrosion, induced grid growth and fractures, as hinted by Valeriote [2].

3.4. Morphology of the corrosion attack

The corrosion attack found with bare grids held at +1200 to +1300 mV versus Hg/Hg_2SO_4 and 80 °C for 11 weeks (equivalent to ~13.5 years at 20 °C) is shown

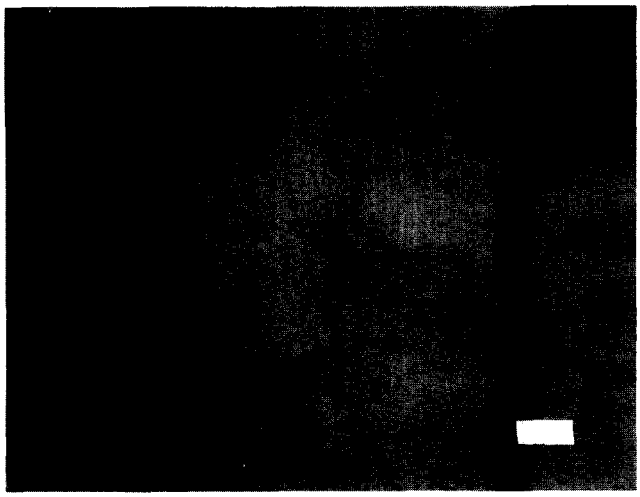

Fig. 16. Microstructure of Pb–Ca–Sn–Al (A707) alloy (reference bar 440 μm). Nominal grid thickness 2.6 mm.

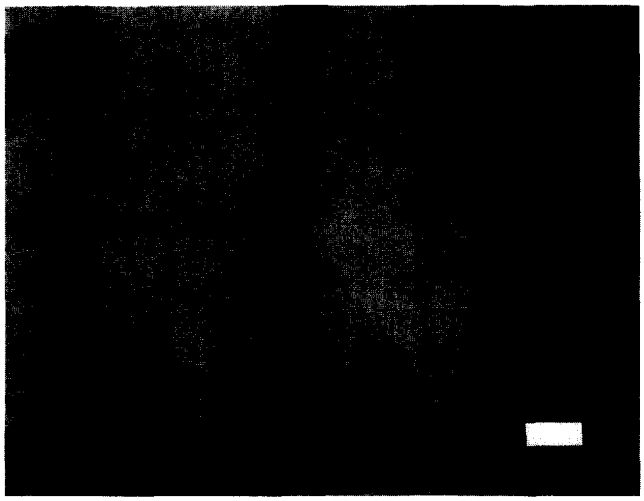

Fig. 17. Microstructure of Pb–Ca–Sn–Al (A707) alloy (reference bar 440 μm). Nominal grid thickness 1.6 mm.

in Figs. 18–21) for diamond-shaped grid members. The attack can be classified as follows.

Pb–Ca–Sn–Al (A903) alloy. Irregular penetrating corrosion attack occurs with a corrosion product thickness of approximately 160 μm (Fig. 18). The attack proceeds along grain boundaries and shows local areas of strong volume-type attack (macro-pitting).

Pb–Ca–Sn–Al (A907) alloy. Very regular corrosion attack is observed without preferred grain boundary attack (Fig. 19). The corrosion product thickness is ~120 μm. There is an absence of locally enhanced volume corrosion (macro-pitting).

Pb–Ca–Sn–Al (A603) alloy. Irregular corrosion attack takes place with locally enhanced volume-type attack (Fig. 20). The observed attack is intermediate between that of the (irregular) A903 and the (smooth) A607 alloy attack. The corrosion product thickness is ~100 μm.

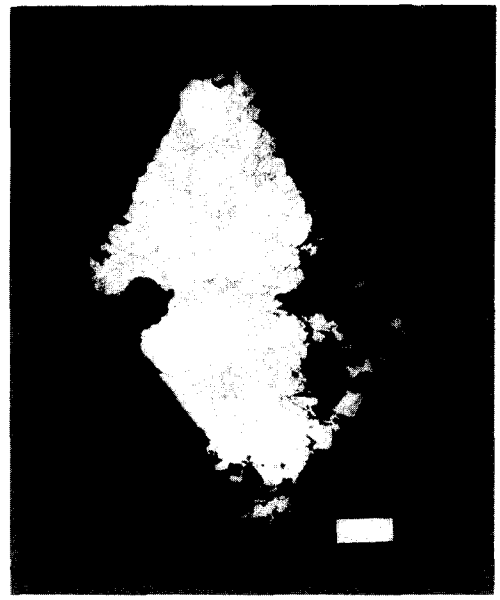

Fig. 18. Corrosion attack of Pb–Ca–Sn–Al (A903) alloy (reference bar 440 μm). Cross section of diamond-shaped interior wire member of the grid. Irregular, penetrating corrosion with localized macro-pitting.

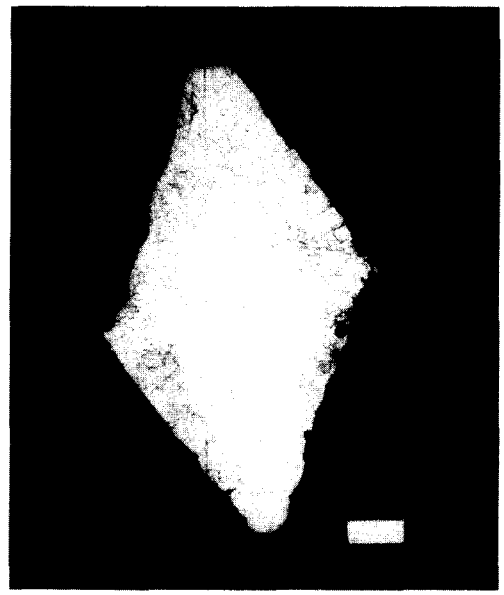

Fig. 19. Corrosion attack of Pb–Ca–Sn–Al (A907) alloy (reference bar 440 μm). Cross section of diamond-shaped interior wire member of the grid. Uniform corrosion without localized macro-pitting.

Pb–Ca–Sn–Al (A607) alloy. Very regular corrosion attack is found without preferred grain boundary attack (Fig. 21). The corrosion product thickness is ~80 μm. There is an absence of locally enhanced volume corrosion (macro-pitting).

From the analysis of the attack types, the action of tin on the macroscopic corrosion morphology can be described as preventing localized, penetrating, macro-pitting corrosion, and also as reducing the volume corrosion of the grid. The reduced attack can be cor-

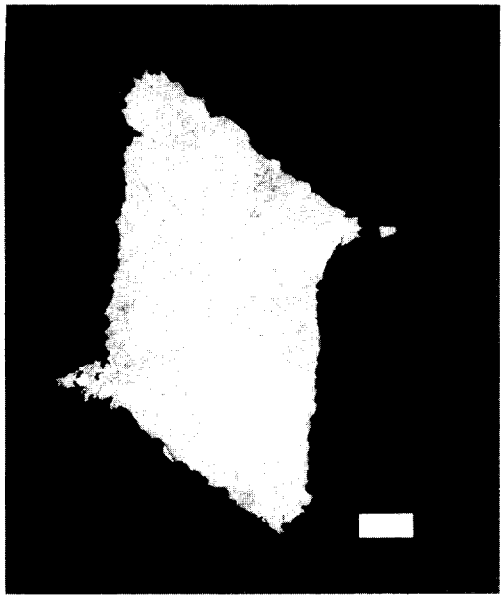

Fig. 20. Corrosion attack of Pb–Ca–Sn–Al (A603) alloy (reference bar 440 μm). Cross section of diamond-shaped interior wire member of the grid. Corrosion attack with minor, localized macro-pitting. Attack is intermediate between (irregular) A903 alloy and (smooth, uniform) A607 alloy attack.

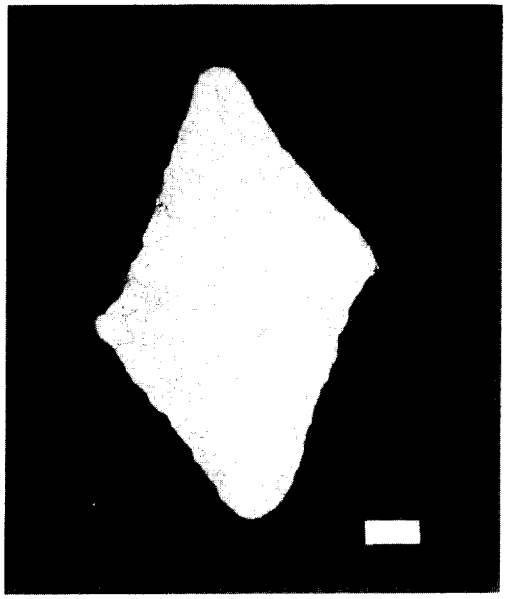

Fig. 21. Corrosion attack of Pb–Ca–Sn–Al (A607) alloy (reference bar 440 μm). Cross section of diamond-shaped interior wire member of the grid. Uniform corrosion attack without localized macro-pitting.

related to the lower number of grain boundaries per unit of volume in low-calcium/high-tin alloys.

3.5. Plate growth results

The bare grid corrosion experiments were complemented with accelerated life-tests of pasted plates in VRLA cells and monoblocs. For this purpose, 4 mm thick grids, cast with the A903 or A707 alloy, were

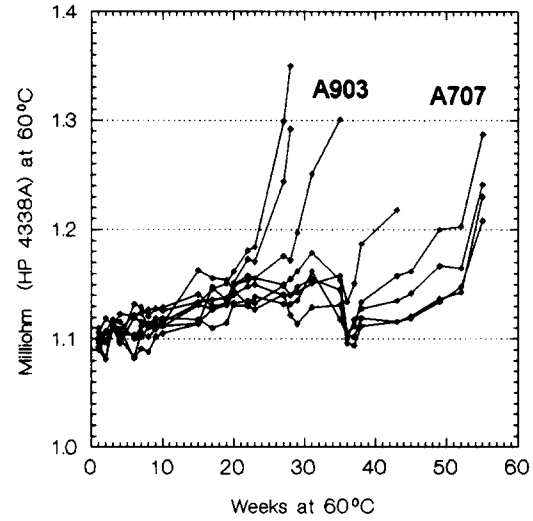

Fig. 22. Plot of internal resistance, in milliohm (HP 4338A), of 4 units of 6 V/100 Ah monoblocs for each tested alloy of A903 and A707 types. Test temperature 60 °C and float voltage 2.28 V/cell. Longest test duration: 54 weeks, equivalent to ~16.6 years at 20 °C.

pasted and formed into positive plates. Positive plates with 20 Ah nominal capacity were used to assemble 6 V/100 Ah (*C*/10 rate to 1.82 V/cell at +20 °C) and 2 V/300 Ah VRLA monoblocs. Positive plates with a nominal capacity of 50 Ah were used to assemble 2 V/450 Ah VRLA cells.

The accelerated life-test was carried out at +60 °C and at a float voltage of 2.28 V/cell. An ageing factor acceleration of 16 was assumed on the basis of the doubling of the ageing speed for every 10 °C above the 20 °C reference temperature (thus, 1 week float at +60 °C corresponds to 16 weeks float at +20 °C). The ageing of the cells and monoblocs was followed by internal resistance measurements and periodic high-rate (10 min/30 min) discharges to 1.60 V/cell at room temperature.

3.6. Internal resistance data

The internal resistance measurements were made with a Hewlett Packard 4338A milliohmmeter (1 KHz, a.c.) with coaxial pin probes at the test temperature of 60 °C and within 5 min after disconnecting the cell or monobloc from the float power supply.

The relevant data obtained with 6 V/100 Ah VRLA monoblocs are shown in Fig. 22. It can be seen that the A903 alloy monoblocs experience a significant and rapid increase in internal resistance (+10%) after 22 to 37 weeks of float. The observed large and undesirable spread of the time, from 23 to 40 weeks to equal end-of-life resistance, correlates also with the observations made with the growth data of bare grids. The monoblocs with the A707 alloy exhibit ~100% longer corrosion life and a more consistent time (51–55 weeks) to equal end-of-life resistance.

Table 2
Capacity of 6 V/100 Ah (C/10) monoblocs, as determined at room temperature with a high rate (10 min) discharge with 277 A to 1.60 V/cell. Discharge time in seconds referenced to +20 °C

Weeks at 60 °C	Alloy type							
	A707/1	A707/2	A707/3	A707/4	A903/1	A903/2	A903/3	A903/4
0	605	599	629	628	601	566	591	565
28						215		163
35	638	635	645	651	152		552	
39	675	692	682	682			295	
43	712	733	717	716				
47	693	659	675	650				
50	725	747	707	707				
54	653	615	547	654				

Table 3
Residual capacity (10 min discharge at 20 °C to 1.60 V/cell) and observed growth of positive plates after dismantling the cells (sample size >20 measurements/test)

Alloy type	Float test duration at 2.28 V/cell	Cell size (Ah)	Capacity at end-of-life 10 min rate (%)	Grid growth (%)
A903	28 weeks (8.6 years at 20 °C)	100	≈31	≈7
A707	52 weeks (16.0 years at 20 °C)	450	>100	≈3
A707	53 weeks (16.3 years at 20 °C)	300	≈65	≈6
A707	54 weeks (16.6 years at 20 °C)	100	>100	≈4

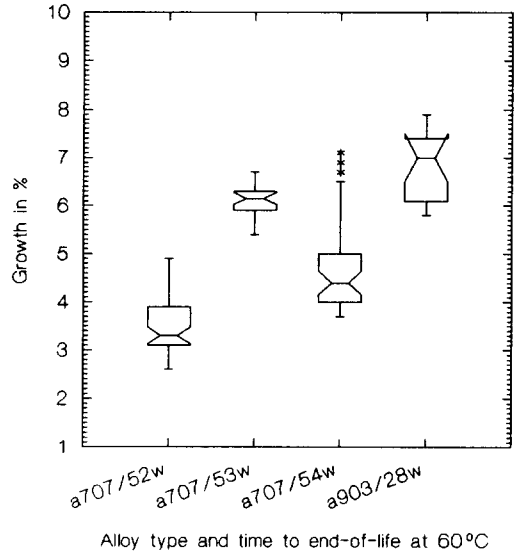

Fig. 23. Notched box plot of the grid growth of pasted grids with A707 and A903 alloys with nominal grid thickness of 4.0 mm (box with 95% confidence intervals). The plates were extracted from cells and monoblocs floated at +60 °C for 28, 52, 53 and 54 weeks and 2.28 V/cell. Residual capacity of the cells and monoblocs at the end of the test were: A707/52 week > 100%; A707/53 week ≈ 65%; A707/54 week > 100%; A903/28 week ≈ 31%.

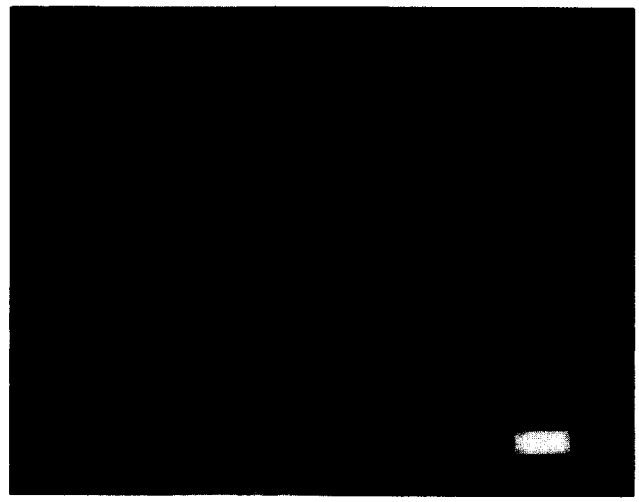

Fig. 24. Microstructure of Pb–Ca–Sn–Al (A903) alloy (reference bar 202 μm). Cross section of triangular interior wire member of the grid. Irregularly-sized grains.

The measurements of internal resistance were used to follow, on a weekly and qualitative basis, the health of the cells and monoblocs. No attempt was made to correlate the milliohm resistance data directly with the residual capacity, and only major and persistent changes of resistance were used as indicators of the health of cells or monoblocs. Cell capacity measurements were made at selected intervals and at moments of significant change in internal resistance.

The test results of a set of four monoblocs per alloy are shown in Table 2. A high-rate discharge test (10/30 min to 1.60 V/cell) was chosen to monitor the

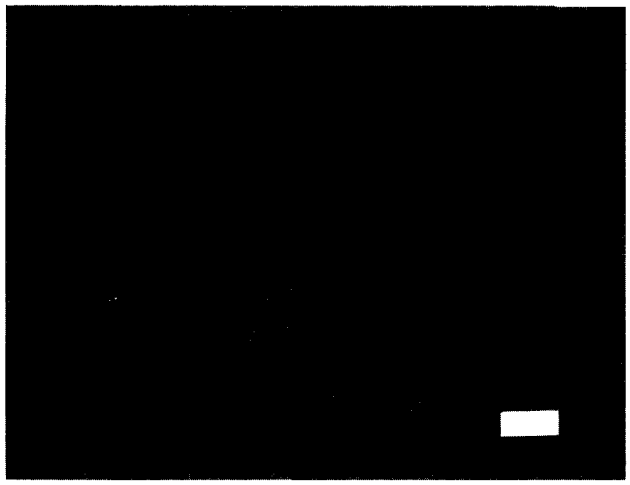

Fig. 25. Details of microstructure of A903 alloy (reference bar 24 μm). Pronounced large areas of rod-like Pb_3Ca precipitate behind moved grain boundaries.

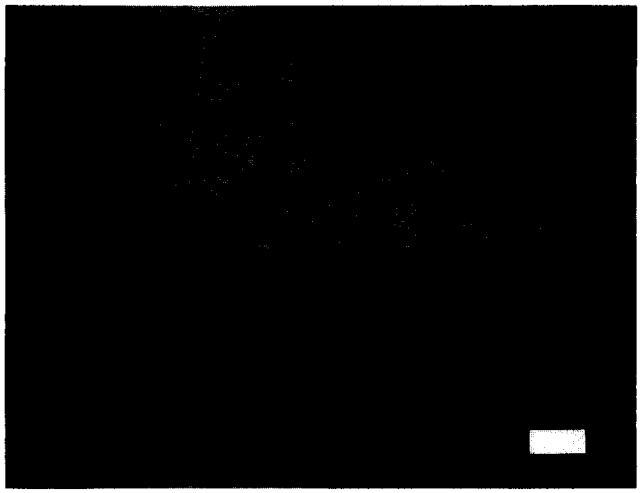

Fig. 26. Microstructure of Pb–Ca–Sn–Al (A707) alloy (reference bar 202 μm). Cross section of triangular interior wire member of the grid. Regular-sized grains with slight orientation effects along heat-flow axis and tin-induced sub-structure.

residual capacity at this condition is particularly sensitive towards changes in the internal resistance of the cells. The 'jumpy' discharge capacity data of the A707 monoblocs after 43 weeks cannot be explained at this stage. It coincided, however, with a variable duration of room temperature float before the capacity test.

In parallel to the above test with 6 V/100 Ah (20 Ah/plate) monoblocs, corrosion life tests were also undertaken with 2 V/300 Ah (20 Ah/plate) and 2 V/450 Ah (50 Ah/plate) units. The same alloy types (namely, A903 and A707) were employed for the manufacture of the positive grids. In both units, a nearly identical differentiation between the corrosion life of A903 grids (28 weeks to rapid rise in internal resistance) and A707 grids with 52–54 weeks to a resistance rise was observed. At intervals, throughout the test, discharges confirmed the residual 10/30 min discharge capacity of the units. The capacity results correlated with the observed rises in resistance.

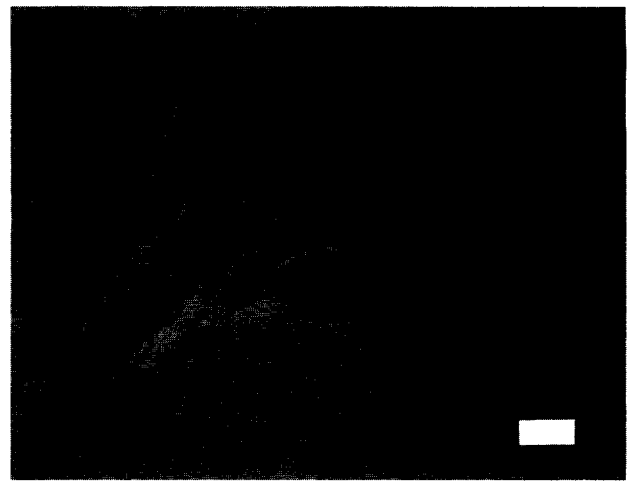

Fig. 27. Details of microstructure of A707 alloy (reference bar 24 μm). Pronounced 'coring' (non-equilibrium solidification) effects. Reduced number of grain boundaries per unit of alloy volume. Small seams containing Pb_3Ca next to moved grain boundaries.

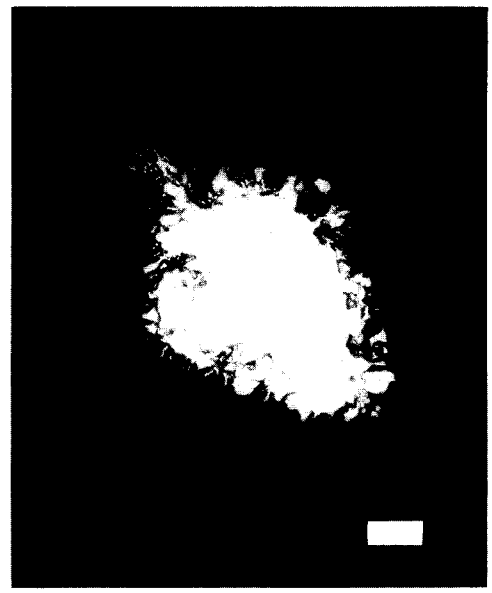

Fig. 28. Microstructure attack of Pb–Ca–Sn–Al (A903) alloy after 28 weeks (end-of-life) float corrosion in VRLA battery held at +60 °C. Localized penetration with bulk oxidation. Diamond-shaped grid member (reference bar 440 μm).

3.7. Grid growth in cell tests

At the end of the float test, the grid growth was determined with plates from selected cells. The sample size was >20 plates per alloy, and the end-of-life time of each tested cell and monobloc size. The growth value was taken as the largest change in horizontal dimension of the particular plate.

Fig. 29. Microstructure attack of Pb–Ca–Sn–Al (A903) alloy after 28 weeks (end-of-life) float corrosion in VRLA battery held at +60 °C. Localized penetration with bulk oxidation. Triangular grid member (reference bar 440 μm).

The data are listed in Table 3 and Fig. 23 and reveal the superiority of the A707 (0.07wt.%Ca–0.7wt.%Sn) alloy over the A903 (0.09wt.%Ca–0.3wt.%Sn) alloy. Also it can be seen that a horizontal grid growth of up to +4% (≈6.2 mm) only minimally impinges upon the high-rate capacity of the employed VRLA cell design. A further growth of ~1.5 mm to +5% (≈7.7 mm) results in significant capacity loss under the applied discharge regime. The larger growth of the A707/53 week plates can be correlated with a high end-of-life float current of ~100 mA/Ah observed in these 300 Ah (C/10) cells, as compared with 5 mA/Ah in the other cells and monoblocs. This higher float current raises the internal temperature of the monobloc and thus promotes an acceleration in the grid growth.

All the grid growth was safely contained within the cell case and no secondary damage or internal shorting was found to occur.

3.8. Pasted plate corrosion morphology

The positive plates from the above test cells, floated for 28 (A903 alloy) and 54 (A707 alloy) weeks were sampled in selected regions in order to determine the corrosion morphology of the alloys under the above VRLA float conditions.

The microstructure of the alloys used in the battery experiment are shown in Figs. 24–27 and exhibit the typical irregularly-shaped grain structure of the A903 Pb–Ca–Sn–Al alloy and the oriented, regularly-shaped A707 Pb–Ca–Sn–Al alloy with a tin-induced sub-grain structure. The cross section is that of a triangular grid member.

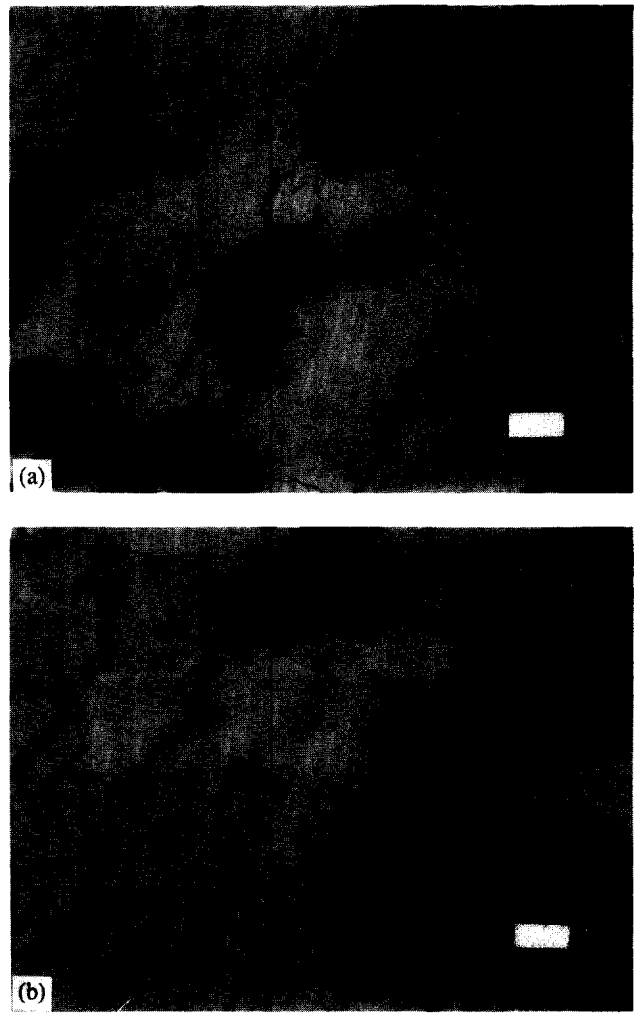

Fig. 30. (a)(b) Details of microstructure attack of Pb–Ca–Sn–Al (A903) alloy after 28 weeks (end-of-life) float corrosion in VRLA battery held at +60 °C. Penetration along grain boundaries followed by hemispherical bulk attack (reference bar 24 μm).

In both alloys, regions of oriented rod-like Pb_3Ca precipitates are found behind the moved grain boundaries. The magnitude of this precipitate is significantly smaller in the A707 alloy and consists only of small rims. Next to the oriented grain-boundary precipitates, there are also several small (<1 μm) isolated and randomly distributed, star-shaped precipitates within the grain. The precise nature/composition has not been determined (Al-containing phase?).

The grids of the positive plates, taken from the test batteries at the respective end-of-life of 28 weeks/60 °C (A903 alloy) and 54 weeks/60 °C (A707 alloy), were investigated for the morphology of the corrosion attack. For this purpose, the active mass was removed and the 'bare' grids were embedded under vacuum with epoxy resin. From these samples, the following observations can be made (Figs. 28–33).

Pb–Ca–Sn–Al (A903) alloy after 28 weeks. Strong corrosion with penetration of up to 400 μm in isolated

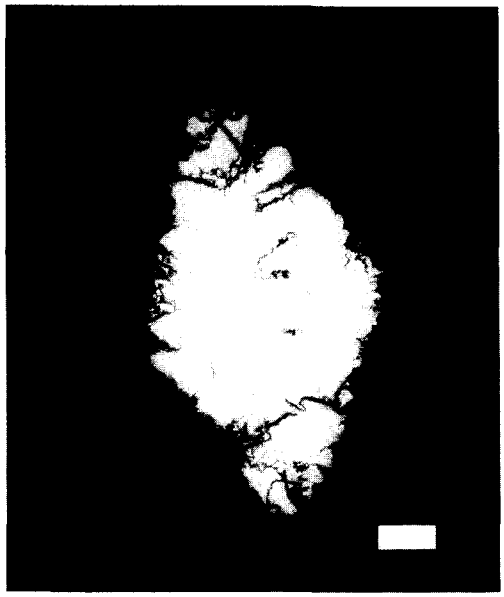

Fig. 31. Microstructure attack of Pb–Ca–Sn–Al (A707) alloy after 54 weeks (end-of-life) float corrosion in VRLA battery held at +60 °C. Severe localized penetration with grain undercutting. Diamond-shaped grid member (reference bar 440 μm).

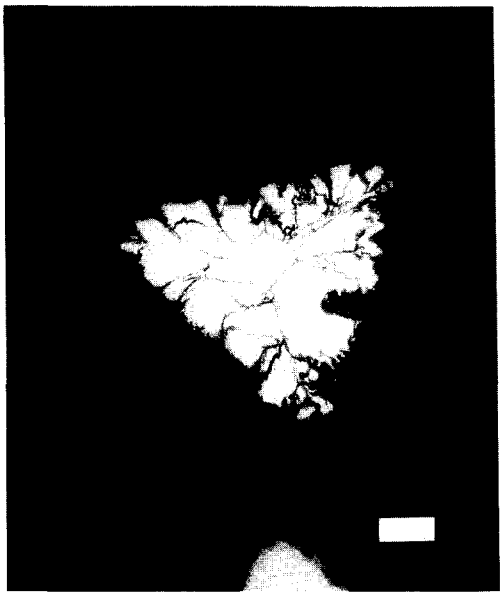

Fig. 32. Microstructure attack of Pb–Ca–Sn–Al (A707) alloy after 54 weeks (end-of-life) float corrosion in VRLA battery held at +60 °C. Severe localized penetration with grain undercutting and complete side-to-side penetration of attack. Triangular grid member (reference bar 440 μm).

points. The corrosion proceeds via the grain boundaries into the interior of the grid, followed by a strong attack of the bulk of these grains with a hemispherical attack front. This bulk attack increases the amount of oxidized lead and contributes to the large growth of the grids cast with this alloy (see Figs. 28–30(a)(b)). No complete, side-to-side penetration of the corrosion front along the grain boundaries was observed.

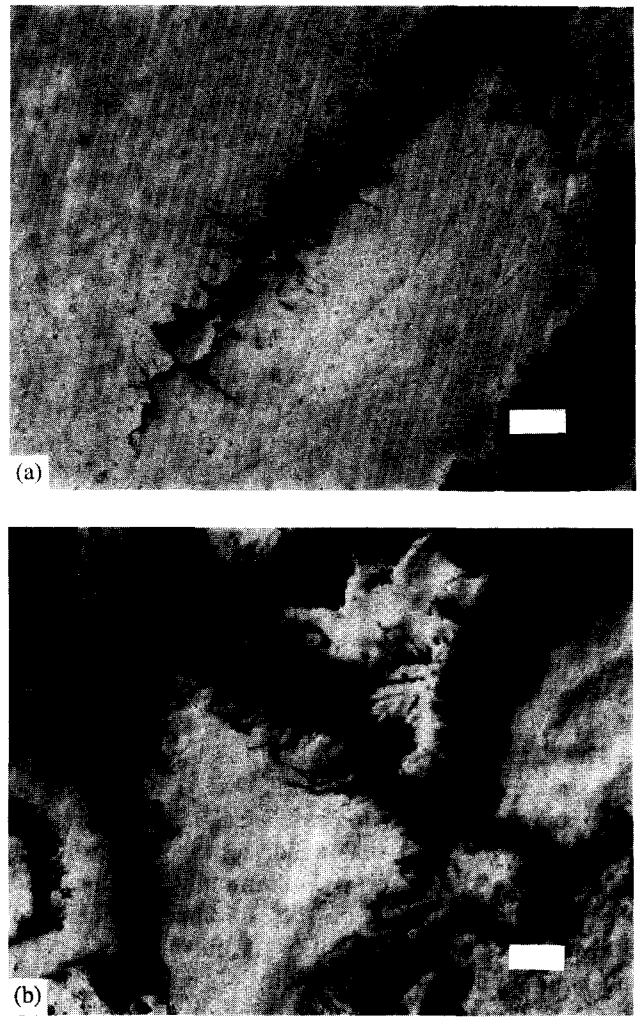

Fig. 33. (a)(b) Details of microstructure attack of Pb–Ca–Sn–Al (A707) alloy after 54 weeks (end-of-life) float corrosion in VRLA battery held at +60 °C. Narrow penetration along grain boundaries followed by slow attack of bulk of grain with a comb-like corrosion front (reference bar 24 μm).

Pb–Ca–Sn–Al (A707) alloy after 54 weeks. Severe intergranular corrosion is visible at the end-of-life (after 54 weeks, i.e., ≈twice of that of the A903 alloy). The penetration of the corrosion front follows preferentially the as-cast-grain boundary. Depending on the cross section of the grid (triangular- or diamond-shaped), a variable number of the alloy grains are completely surrounded by a corroded grain boundary (see Figs. 31 and 32). The corrosion of the bulk of the grain occurs in a slower fashion than that observed with the A903 alloy. The corrosion, moving from the grain boundary into the bulk of the grain, often shows a comb-like front. This probably replicates the local microstructure of the alloy in the vicinity of the boundary.

The details of these attack types are shown in Figs. 28–33(a)(b). When comparing the attack type morphology, little difference is noted between the attack of bare and pasted grids with the A903 alloy. With the

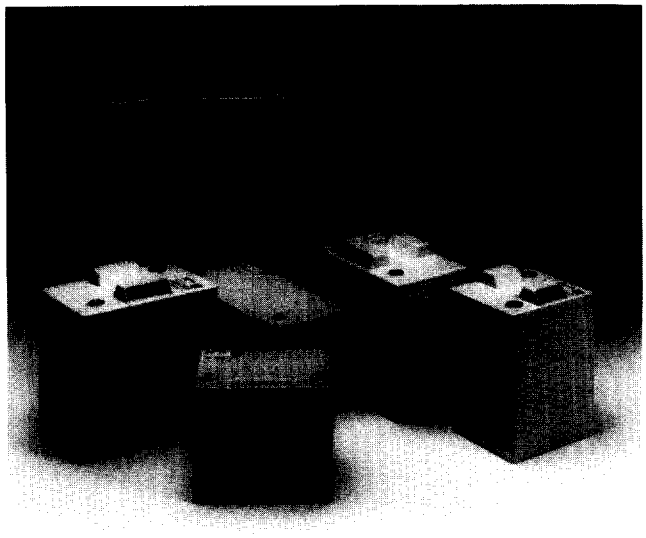

Fig. 34. +plus Oerlikon Compact Power™ VRLA cells and monoblocs.

A707 alloy, the corrosion attack of bare grids proceeds in a uniform fashion without any pronounced grain-boundary attack. With pasted grids (i.e., plates), a strong sensitivity towards enhanced grain-boundary attack is noted.

4. Conclusions

1. The test results, obtained with bare and pasted grids, show that Pb–Ca–Sn alloy compositions, with a low number of grain boundaries per unit volume or surface, have a superior corrosion resistance, i.e., low grid growth. Tin is the predominant element in enhancing the corrosion resistance of these grid alloys.
2. From the above data, large-grained alloys with the composition 0.07wt.%Ca–0.7wt.%Sn are desirable for long-life VRLA batteries (see Fig. 34).
3. The corrosion of the grids can be monitored efficiently through the measurement of the internal resistance (1 KHz, a.c.) of the batteries.

Acknowledgement

The author thanks Mr A. Matteo for setting-up and supervising the corrosion experiments.

References

[1] R. McGill, J.W. Tukey and W.A. Larsen, *Am. Stat., 32* (1978) 12.
[2] E. Valeriote, D. Kelly and P. Niessen, *J. Electrochem. Soc., 132* (1985) 1783.